Nano artificial periosteum PLGA/MgO/Quercetin accelerates repair of bone defects through promoting osteogenic − angiogenic coupling effect via Wnt/ β-catenin pathway

Xi He [a,b], Wenbin Liu [b,c,**], Yanling Liu [d], Kai Zhang [b,c], Yan Sun [b,c], Pengfei Lei [b,c,e,***], Yihe Hu [a,b,c,e,*]

[a] Department of Sports Medicine, National Clinical Research Center for Geriatric Disorders, Xiangya Hospital, Central South University, Changsha, China
[b] Hunan Engineering Research Center of Biomedical Metal and Ceramic Implants, Changsha, China
[c] Department of Orthopedic Surgery, National Clinical Research Center for Geriatric Disorders, Xiangya Hospital, Central South University, Changsha, China
[d] Provincial Laboratory for Diagnosis and Treatment of Genitourinary System Disease, Department of Urology, Xiangya Hospital, Central South University, Changsha, China
[e] Department of Orthopedics, The First Affiliated Hospital, Medical College of Zhejiang University, Hangzhou, China

ARTICLE INFO

ABSTRACT

Bone nonunion or delayed union, caused by stripping or injuring of periosteum, is the most common sequelae of segmental bone defects. The preservation of periosteum, or the use of periosteal grafts, can significantly improve the integration of bone graft, speeding up the process of bone reconstruction. However, in most cases, periosteum cannot be preserved with bioactivity. Thus, it is pivotal to develop artificial periosteum. In this study, artificial periosteum of PLGA/MgO/Quercetin was prepared by electrospinning. PLGA/MgO/Quercetin membranes were shown to have a highly porous surface and microstructure, as observed by scanning electron microscopy. Along with excellent biocompatibility, PLGA/MgO/Quercetin membranes promoted cell proliferation and migration, as well as osteogenic differentiation of BMSCs (Bone marrow mesenchymal stem cells) in a dose-dependent manner through the activation of Wnt/β-Catenin pathway. The PLGA/MgO/Quercetin membranes, with an appropriate concentration of quercetin (<1 wt%), promoted EPCs (Endothelial progenitor cells) angiogenesis. In a subcutaneous implantation model and rat skull defect model, optimal osteogenesis and angiogenesis function were observed for the PLGA/20 wt% MgO/0.1 wt% Quercetin membrane. In conclusion, PLGA/MgO membranes, with an appropriate concentration of quercetin, show a variety of biological activities and are promising materials for the generation of artificial periosteum.

1. Introduction

Segmental bone defects caused by trauma, tumor resection, and congenital malformation are major clinical problems. In the treatment of segmental bone defects, timely and abundant vascular growth helps to achieve good prognosis [1,2]. Clinical and experimental data show that the growth of blood vessels is closely related to periosteum, a highly vascularized dense membrane surrounding the bone cortex, providing cellular and nutritional support for osteogenesis. The vascular network also promotes rapid bone regeneration [3]. One of the most common

problems associated with the treatment of segmental bone defects is bone nonunion or delayed healing, which is usually related to the stripping or injury of periosteum. However, the preservation of periosteum, or the usage of periosteal grafts, can significantly improve the integration of bone grafts, accelerating the reconstruction process [4–6]. Due to the pivotal function of periosteum in bone healing and remodeling, as well as the high demand for periosteum in orthopedic surgery, it is necessary to develop artificial periosteum.

Nanofiber membranes prepared by electrospinning are a promising artificial periosteum, owing to their similarity to the extracellular matrix

and periosteum structure; this helps to induce osteoblast adhesion, proliferation, differentiation, mineralization, and neovascularization [7–10]. Biomaterials prepared by electrospinning have been proved to promote critical-size bone defect repair [11]. Bone tissue scaffolds prepared by electrospinning of poly (lactic-co-glycolic acid) (PLGA) and bioceramics have been shown to have excellent biocompatibility and biodegradability. PLGA scaffolds with magnesium oxide (MgO) promoted osteogenesis by sustained release of Mg^{2+} [12–14]. MgO nanoparticles have also been shown to promote bone regeneration and angiogenesis [15,16].

Quercetin (Que) is one of the flavonoid substances extracted from Chinese herbal medicine and fruits. Que has a variety of biological activities and has shown effectiveness as a neuroprotective, anti-histamine, anti-oxidant, anti-inflammatory, anti-microbial and anti-tumor [17]. Que has also been shown to participate in the maintenance of bone homeostasis. Que can inhibit RANKL mediated osteoclastogenesis, osteoblast apoptosis, oxidative stress and inflammation. In addition, Que can promote osteogenesis, antioxidation, adipocyte apoptosis and osteoclast apoptosis by regulating Wnt and NF-κB, Nrf2, Smad-dependent, as well as intrinsic and extrinsic apoptotic pathways [18]. Further, Que regulates the expression of osteogenic related genes (such as Runx2 and OPN), promoting the osteogenic differentiation of stem cells [18–21]. Through MAPK and Wnt/β-Catenin signaling pathways, Que inhibits LPS induced apoptosis and enhances osteogenic differentiation in MC3T3-E1 cells [22]. Que also improves osteoporosis in ovariectomized rat by enhancing osteogenic ability of rat stem cells [22,23]. Flavonoid has been reported to prevent bone loss by upregulating signaling pathways which promoting osteoblast function [24,25]. Another flavonoid derived from Chinese herbal extracts, Icariin showed synergistic effect with MgO on induced osteogenesis [13]. Que in magnesium-doped calcium silicate ceramic showed better osteogenesis function than magnesium-doped calcium silicate ceramic as well as calcium silicate ceramic [26]. Thus, we assumed that Que, a bioflavonoid compound, might show synergism effect with MgO on osteogenesis. However, there is a lack of research on artificial periosteum loading Que together with MgO and more evidence is required for Que enhanced bone regeneration with MgO.

In this study, nano artificial periosteum of PLGA/MgO/Que were prepared using an electrospinning process, and the efficacy of these materials in bone regeneration was assessed.

2. . Materials and methods

2.1. Materials

PLGA (Mw = 120,000 Da) was purchased from Sigma-Aldrich. Quercetin was purchased from Sinopharm Chemical Reagent Co., Ltd. (China). MgO nanoparticles and dimethylformamide (DMF) solvent and acetone were obtained from Aladdin. Other analytically pure reagents were used without further purification.

2.2. Preparation of PLGA/MgO/Quercetin artificial periosteum

To prepare electrospinning solutions, PLGA, MgO and Que were dissolved in 4 mL DMF and 4 mL acetone, in different concentrations (Table S1). The initial weight feeding ratio of PLGA/MgO was 1:0.2 (w:w) [12,13,27], and the spinning solution was loaded into a 10 mL syringe and fixed on the pusher. The distance between the needle tip of the syringe and the collecting plate was 10 cm. Additional spinning parameters were as follows: positive voltage 12 kV, negative voltage 2 kV, pushing speed 0.3 mL/h, collecting drum speed 100 rpm. The electrospinning membranes of PLGA/quercetin with mass ratio of 0.01%, 0.1% and 1% were prepared. These were named PLGA/20 wt% MgO as PLGA/MgO, PLGA/20 wt%MgO/0.01 wt%Que as 0.01% Que, PLGA/20 wt%MgO/0.1 wt%Que as 0.1% Que, PLGA/20 wt%MgO/1 wt%Que as 1% Que in following illustrations.

2.3. Characterization

The morphology of PLGA/MgO/Que was characterized by scanning electron microscopy (SEM) (Zeiss SIGMA, UK). The electrostatic spinning film was cut into 5 mm × 5 mm size and then sprayed with gold before SEM observation.

The hydrophilic and hydrophobic properties of the PLGA/MgO/Que surface were measured with a water contact angle meter (JC2000C 50Hz KRUSS Germany). 10 μL of deionized water was dropped onto the PLGA/MgO/Que surface to keep it smooth and flat. At least three different positions of each material were measured and averaged after multiple measurements.

Fourier transform infrared spectroscopy (FTIR, Nicolet 6700 Spectrophotometer) was used to measure and analyze the group changes of PLGA/MgO/Que. The procedure was film method, and the size of nanofiber film was detected as 5 mm × 5 mm. The scanning spectral range was 4000 cm^{-1}-400 cm^{-1}, and the resolution was 4 cm^{-1}.

To study the ion release of MgO in nanofibers, the ion concentration was determined by inductively coupled plasma emission spectrometry. (ICP-OES,LeemanLabs,USA). A 10 mg fiber membrane was immersed in a 1 mL centrifuge tube containing an equal amount of PBS (PH = 7.4) buffer and aged at 37 °C for 1,3,5,7,9 and 14 days on a horizontal oscillator (Guohua Enterprises SHA-C). The PBS buffer (1 mL) was collected and centrifuged at 10000 rpm for 10 min. The concentrations of magnesium ions in the solution were measured by ICP-OES.

2.4. Animals

6–8 week age male Sprague-Dawley (SD) rats were used to construct cranial defecting models and subcutaneous angiogenesis models. Male SD rats (60–80 g) were used for cell isolation. All animal experiments were carried out in accordance with the guidelines of the Animal Care and Use Committee of the Central South University and under the ethical approval for research involving animals of Central South University.

After 8 weeks of operation, SD rats were euthanized, and the calvarial specimens were collected and subsequently fixed with 4% paraformaldehyde for further study. Micro-CT (SkyScan, SkyScan1176, Belgium) is first used to assess regeneration conditions in the defect area. The three-dimensional structure of the calvarial was reconstructed by mimic software. Bone volume and Bone volume/tissue volume were calculated by the software.

2.5. Cell culture

BMSC cells were isolated from rats (60–80 g) femur and tibia. BMSC was cultured in α-MEM with 10% FBS and 1% streptomycin-penicillin. BMSC was subcultured at 90% confluency and passage 2–3 BMSC were used for experiments. For osteogenic differentiation, cells were cultured with osteogenic media (MUXMT-90021, Cyagen, Guangzhou, China) for 14–21 days, and the media was replaced every 2 days. Endothelial Progenitor Cells (EPCs) were isolated as described previously [28]. EPCs were cultured in M199 with 10% FBS and 1% streptomycin-penicillin.

Artificial periosteal extracts were obtained by immersing 1 cm^2 artificial periosteal into 10 mL complete media (5% CO_2, 37 °C) and shaking for 24 h (150 rpm). Immersing extracts were used in the following osteogenesis and angiogenesis experiments.

2.6. Transwell migration assay

Transwell migration assay was performed using transwell inserts (NEST) with a filter of 8 μm pore. 1.5×10^4 cells in serum-free media were seeded into the upper chamber of the insert and media (including immersing extracts) were added to the lower chamber. After 12 h of incubation, the cells were fixed with methanol and stained with Crystal Violet Stain. Then, cells on the top surface of the membrane were wiped off, and cells on the lower surface were examined with a Leica

microscope (DM3000). 9 random fields were photographed for counting purposes and the average number of migrated cells was used as a measure of migration capacity.

2.7. Immunofluorescence staining and immunoblotting

Immunofluorescence staining and immunoblotting were conducted as described previously [29]. For Phalloidin/DAPI Staining, cells were fixed 3 days after plating with 4% PFA. After incubating with 5% BSA in 0.1% PBST for 1 h, 1/200 diluted Phalloidin were applied and incubated for 0.5 h at room temperature (RT). After washing three times with PBS, cells were stained with DAPI for 10 min at RT. Subsequently, the cells were washed three times with PBS. Images were taken using confocal scanning microscopy (Leica TCS SP8 X, Germany).

For the cellular immunofluorescence staining of Collagen I and OPN, cells were fixed 3 days after plating with 4% PFA. After incubating with 5% BSA in 0.1% PBST for 1 h, 1/100 diluted primary antibody collagen I (ab260043Abcam, USA) and OPN (ab63856, Abcam, USA) were applied and incubated overnight at 4 °C. 1/200 diluted Goat anti-Rabbit IgG (H + L) Cross-Adsorbed Secondary Antibody 488 were used and incubated for 1 h at RT. After washing three times with PBS, cells were stained with DAPI for 10 min at RT. Subsequently, the cells were washed three times with PBS. Images were taken using confocal scanning microscopy (Zeiss).

For immunoblotting, the protein aliquots, resolved in NP40 lysis buffer, were separated by gel electrophoresis in 10% polyacrylamide mini-gels and were transferred onto a polyvinylidene difluoride (PVDF) film. After incubation with antibodies overnight in 4 °C, Western blot analysis of the protein levels was performed using antibodies including Collagen I (ab260043, Abcam, USA), Runx2 (AF5186, affinity), GAPDH (ab8245, Abcam, USA), and Non-phospho (Active) β-Catenin (8814, CST). Secondary antibodies, including Goat Anti-Rabbit (115-035-146, Jackson ImmunoResearch, USA) and Goat Anti-Mouse IgG (111-035-144, Jackson ImmunoResearch, USA) were applied. West Femto Maximum Sensitivity Substrate (34094, Thermofisher, USA) was used to visualize the results. Biorad ChemiDoc system was used for imaging. Image J was used to export grey density analysis.

2.8. Histological analysis

The harvested specimens were fixed and decalcified in 10% decalcifying solution for 3 weeks at room temperature, followed by alcohol gradient dehydration and embedding in a paraffin block. The embedded specimens were cut into 5 μm-thick histological sections across the center of the defect area and stained with H&E or Masson to evaluate the regeneration condition.

For DAB or immunofluorescence staining, the sections were prepared for antigen restoration by immersion in 5% hydrogen peroxidase and blocked with BSA containing 0.1% Triton X-100 for 1 h (h) at room temperature. Subsequently, they were incubated overnight at 4 °C with primary antibodies against CD31 (1:500), β3-tubulin (1:100), OCN (1:500), then incubated with HRP-conjugated secondary antibodies and counterstained with hematoxylin or corresponded fluorescence secondary antibodies. Additionally, 1% DAPI was used to stain the cell nuclei. Finally, all the images were taken under a microscope (Leica DM3000).

2.9. Cell proliferation analysis and live/dead cell staining

1×10^4 cells (BMSCs and EPCs) were plated in 96-well plates and cultured with immersing extracts for 1 and 3 days. Cell proliferation was analyzed by Cell Counting Kit-8 (Beyotime), according to manufacturer's instruction at 450 nm using microplate readers (Molecular Devices).

BMSCs were cultured in 24-well plates. Calcein-AM/PI double staining was conducted using Calcein-AM/PI double stain kit after 24 h of culturing in immersing extracts. This kit provides two molecular probes: Calcein-AM one probe labels the living cells as green and the PI probe simultaneously labels the dead cells as red. The results were observed using confocal microscopy.

2.10. Alizarin red S staining and ALP staining

For Alizarin red S staining, BMSCs cultured in osteogenic media for 14 days were fixed with 4% PFA and stained with 0.2% Alizarin red S solution for 0.5 h, then washed with ddH$_2$O for 3 times.

For ALP staining, BMSCs cultured in osteogenic media for 3 days were fixed with 4% PFA and stained with BCIP/NBT Alkaline Phosphatase Color Development Kit (beyotime) for 0.5 h and then washed with PBS (×3).

2.11. Tube formation assay

Matrigel was thawed on ice overnight. 110 μL of Matrigel (#356231, Corning) was added per well (48-wells plates) and allowed to polymerize for 30 min at 37 °C. For each well, 2.5×10^4 cells were plated and observed at 3 and 6 h. After staining with Calcein-AM, cells were also observed under microscope. Tube formation was analyzed by counting total nodes, total branches, and measuring branch length with ImageJ.

2.12. Gene expression analysis

Quantitative PCR was applied to detect the expression of certain genes. Total RNA was isolated using Trizol reagent (Invitrogen, USA). A total of 1000 ng RNA were reverse transcribed using First Strand cDNA Synthesis Kit (Thermofisher, USA). SYBR green PCR Master Mix (Thermofisher, USA) was used in qPCR with CFX96 Connect Real-Time PCR Detection System (BIO-RAD, USA). ΔΔCt method was applied to calculate the results. The primers used in this study were designed by Primer 3.0 (Table S2).

2.13. Statistical analysis

GraphPad statistical software was used to analyze all the data. One-way or two-way analysis of variance (ANOVA) was used to compare experimental data among groups. The difference was considered statistically significant at $p < 0.05$.

3. Results

3.1. The characteristics of PLGA/MgO/Quercetin membranes

The surface morphology of each membrane characterized by SEM showed that the nano spinning fiber membrane of PLGA substrate was irregularly crosslinked by nano fibers, and there was a porous structure between spinning, forming highly porous surface and microstructure (Fig. 1A).

The water contact angle of PLGA/MgO/Que membranes were 113.7 ± 1.897° (PLGA), 118 ± 1.268° (PLGA/MgO), 118.4 ± 3.066° (0.01% Que), 116.7 ± 1.929° (0.1% Que), 117.8 ± 0.832° (1% Que). Membranes loaded with MgO showed increased water contact angles ($p < 0.05$), resulting in worse hydrophilicity compared with PLGA membranes. However, there was no difference between Que loaded membranes (Fig. 1B and C).

Methyl vibration peak in FTIR of PLGA located in 1450 cm^{-1}and 1755 cm^{-1} was the stretching vibration peak of C=O, and 1089 cm^{-1} was the stretching vibration peak of C–O. FTIR of pure Que showed absorption peaks at 3386 cm^{-1},1612 cm^{-1}, 1379 cm^{-1}, 1244 cm^{-1}, which corresponding to the stretching vibration peak of phenolic hydroxyl group, the stretching vibration peak of C=O, the stretching vibration peak of aromatic C–O bond and the stretching vibration peak of C–O–C, respectively. Three characteristic absorption peaks of PLGA were observed in different membranes. We also observed characteristic absorption peaks of Que at 1612 cm^{-1}, 1379 cm^{-1}, 1244 cm^{-1} in Que loaded membranes. The absorption peak of quercetin is more obvious
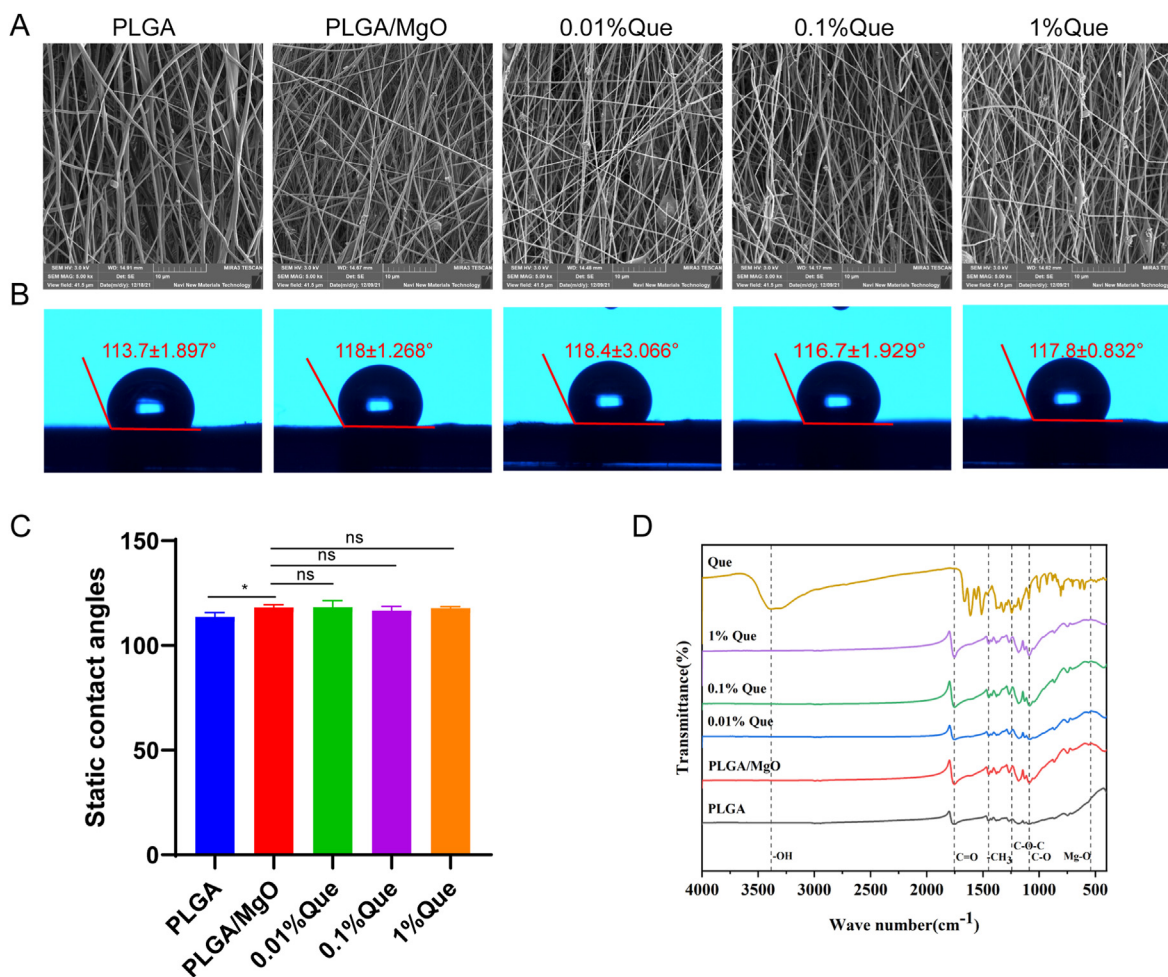
Fig. 1. Characteristics of PLGA/MgO/Que membranes. (A) PLGA/MgO/Que showed highly porous surface and microstructure were observed by SEM; (B) Water contact angle of PLGA/MgO/Que; (C) Compared with PLGA, PLGA/MgO/Que showed increasing contact angles; (D) FTIR of PLGA/MgO/Que; *$p < 0.05$, **$p < 0.01$, ***$p < 0.001$, ****$p < 0.0001$.

with the increase of quercetin addition, which indicating a successful loading of Que. According to previous study [30], we observed absorption peaks of MgO in 540 cm^{-1} which indicating a loading of MgO (Fig. 1D).

Subsequently, we conducted Mg^{2+} release curve on PLGA/MgO, 0.01% and 0.1%Que membranes. Three groups of artificial periosteum could release magnesium ions for more than 14 days. The release curve curves of the three groups were similar, and there was no significant difference among the three groups (Figure S1).

3.2. Cell compatibility

To demonstrate biosafety of artificial periosteum, BMSCs and EPCs were cultured with artificial periosteum immersing extracts. By using Calcein AM (marker of live cells) and PI (marker of dead cells) probes, the ratio of live cells showed no difference ($p > 0.05$) among diverse groups, which indicating that all of the membranes were free of cytotoxins (Fig. 2A and B).

By using CCK8 assay, artificial periosteum immersing extracts were found not to inhibit the proliferation of BMSCs. Increasing proliferation was observed in 0.01%Que artificial periosteum extracts cultured BMSCs within 24 h, compared with PLGA/MgO extracts ($p < 0.05$). Further culturing BMSCs for 72 h, compared with PLGA/MgO, extracts of artificial periosteum loaded with Que showed increasing proliferation

(especially for 0.1% Que and 1% Que films extracts ($p < 0.001$ and $p < 0.01$)) (Fig. 2C). Similar phenotypes were observed in EPCs. Compared with PLGA/MgO, 0.01%Que showed no promoted proliferation in 24 h ($p > 0.05$), however, it showed increasing proliferation within 72 h ($p < 0.01$). 0.1% Que promoted proliferation within 24 and 72 h ($p < 0.05$ and $p < 0.001$). However, 1% Que membranes inhibited EPCs proliferation, compared with PLGA/MgO ($p < 0.05$) (Fig. 2D). It is suggested that the artificial periosteum loaded with 0.01% Que and 0.1% Que can promote the proliferation of cells, which might show better repairing function in fractures or bone defects.

3.3. PLGA/MgO/Que promoted cell migrations

A transwell chamber was used to detect BMSCs and EPCs migrations cultured with diverse artificial periosteum. In BMSCs, PLGA/MgO promoted cell migration compared with PLGA, while artificial periosteum loaded with 0.01% and 0.1% Que promoted cell migration more than PLGA/MgO ($p < 0.05$ and $p < 0.0001$, respectively) (Fig. 3A and C). In EPCs, 0.1% Que promoted cell migrations more than PLGA/MgO ($p < 0.001$) (Fig. 3B and D). 0.01% Que also showed promoted cell migrations although without statistical significance. This was consistent with the results of the CCK-8 assay. 0.01% and 0.1% Que significantly promoted the migration of BMSCs and EPCs, indicating more recruitment of local stem cells and vascular endothelial cells to the fracture site.
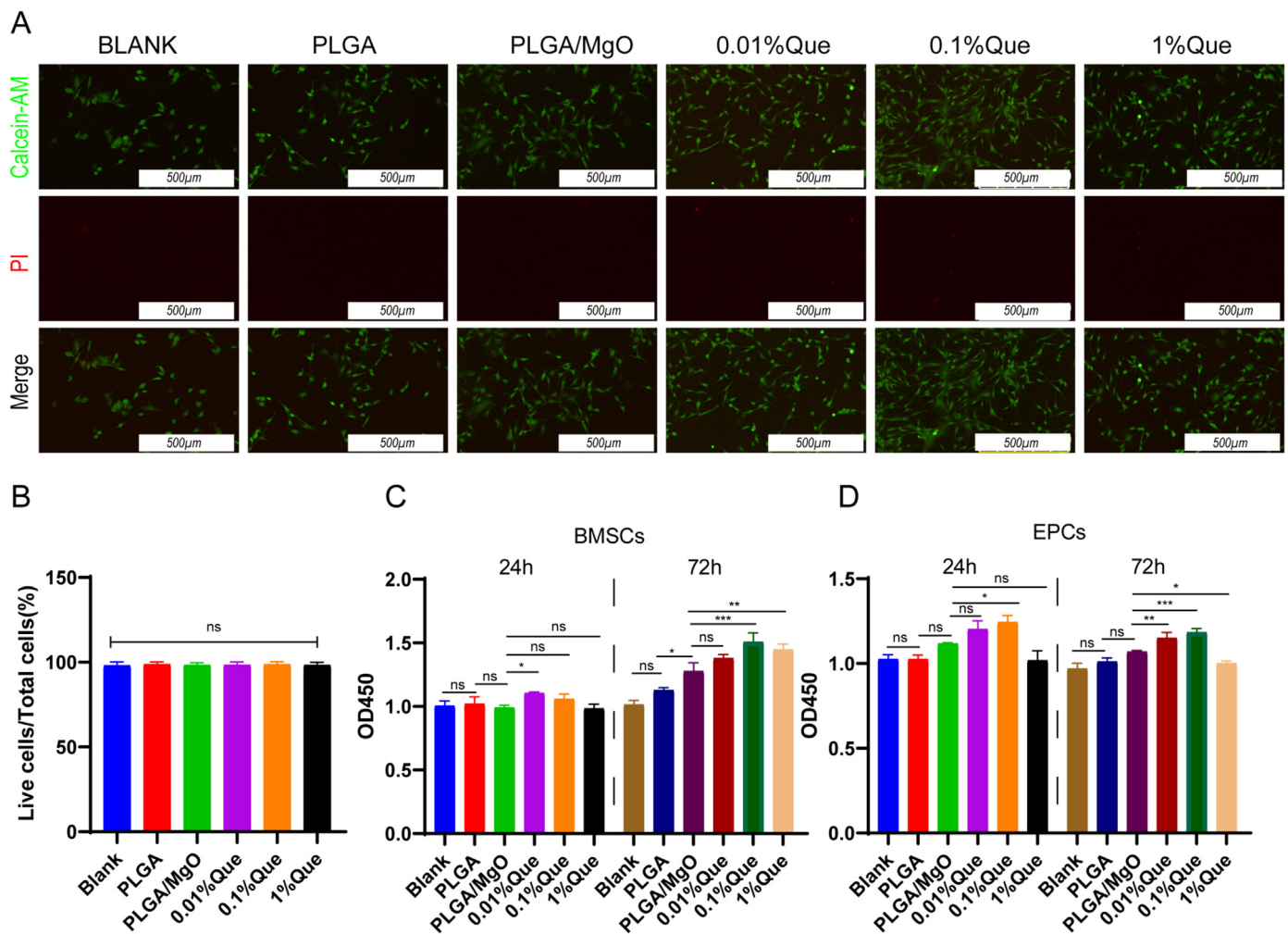
Fig. 2. Biological compatibility of PLGA/MgO/Que. (A) Cultured in membranes immersing extracts, immunofluorescent stained showed live cells (Calcein-AM, in green) and rare dead cells (PI, in red); (B) The ratio of live cells showed no statistically significance among groups; (C) Cell viability assays by CCK-8, Que membranes immersing extracts showed promotion of cell proliferation in BMSCs as well as in EPCs (D); *$p < 0.05$, **$p < 0.01$, ***$p < 0.001$, ****$p < 0.0001$.

3.4. PLGA/MgO/Que increased osteogenesis via Wnt/β-catenin signaling pathway

To clarify the effect of artificial periosteum on osteogenic differentiation, BMSCs were cultured in osteogenic media with extracts. After culturing for 12 days, the expression of osteogenesis related genes was detected by qPCR. Compared with PLGA, PLGA/MgO showed increased expression of Runx2 ($p < 0.0001$), Col1a1 ($p < 0.05$), and Opn ($p < 0.0001$), consistent with a previous study showing that MgO promoted osteogenesis. Compared with PLGA/MgO, the positive control of osteogenesis, 0.01% Que and 0.1% Que increased the expression of Runx2, Alp, Bmp2, Col1a1 and Opn. However, compared with PLGA/MgO, 1% Que only increased the expression of Runx2 ($p < 0.05$) and Col1a1 ($p < 0.05$) (Fig. 4A). We also observed increasing expression of Collagen I and Runx2 by immunoblotting. 0.1% Que showed the highest expression of Collagen I and Runx2 (Fig. 4B). Further study of Alizarin Red stain and ALP Stain were applied to evaluate putative osteogenesis functions of artificial periosteum (Fig. 4C). In both staining, 0.01% and 0.1% Que showed deeper color, indicating more calcium deposition and ALP expression. However, 1% Que showed inhibition of osteogenesis. Through immunofluorescence staining, 0.1% Que also showed the best cell morphology and strongest fluorescence intensity of Collagen I and OPN (Fig. 4D and E). Artificial periosteum loaded with Que promoted osteogenesis and 0.1% Que displayed superior osteogenesis effects

compared with others, suggesting that an appropriate concentration of Que might increase the osteogenesis function of MgO.

Considering the pivotal roles of Wnt/β-catenin in bone repairing, we detected the expression of this pathway. By immunoblotting, we found that PLGA/MgO, 0.01% Que and 0.1% Que showed increasing expression of non-phospho catenin compared with PLGA, and 0.1% Que showed the highest expression level (Fig. 4G). Similar results were observed within the expression of Wnt3a, in which 0.1% Que showed the highest expression ($p < 0.001$ compared with PLGA/MgO), suggesting that 0.1% Que could activate Wnt3a/β-catenin (Fig. 4F).

3.5. PLGA/MgO/Que increased angiogenesis

By analyzing total nodes, total branches and branch lengths in EPCs, we evaluated tube formation in vitro. By culturing in diverse artificial periosteum extract media for 3 h, we observed no difference among the groups. By culturing in diverse artificial periosteum extract media for 6 h, 0.1%Que showed the most total nodes compared with PLGA ($p < 0.05$). 0.1%Que showed the highest total branches ($p < 0.01$) and branching length ($p < 0.05$), compared with PLGA/MgO in 6 h. However, 1% Que showed decreasing total nodes, total branches and branching lengths (Fig. 5A and B). In vitro culturing suggested 0.1% promote angiogenesis.

Additionally, we detected the expression of angiogenesis associated genes including Vegfa and Vwf. Compared with PLGA, PLGA/MgO
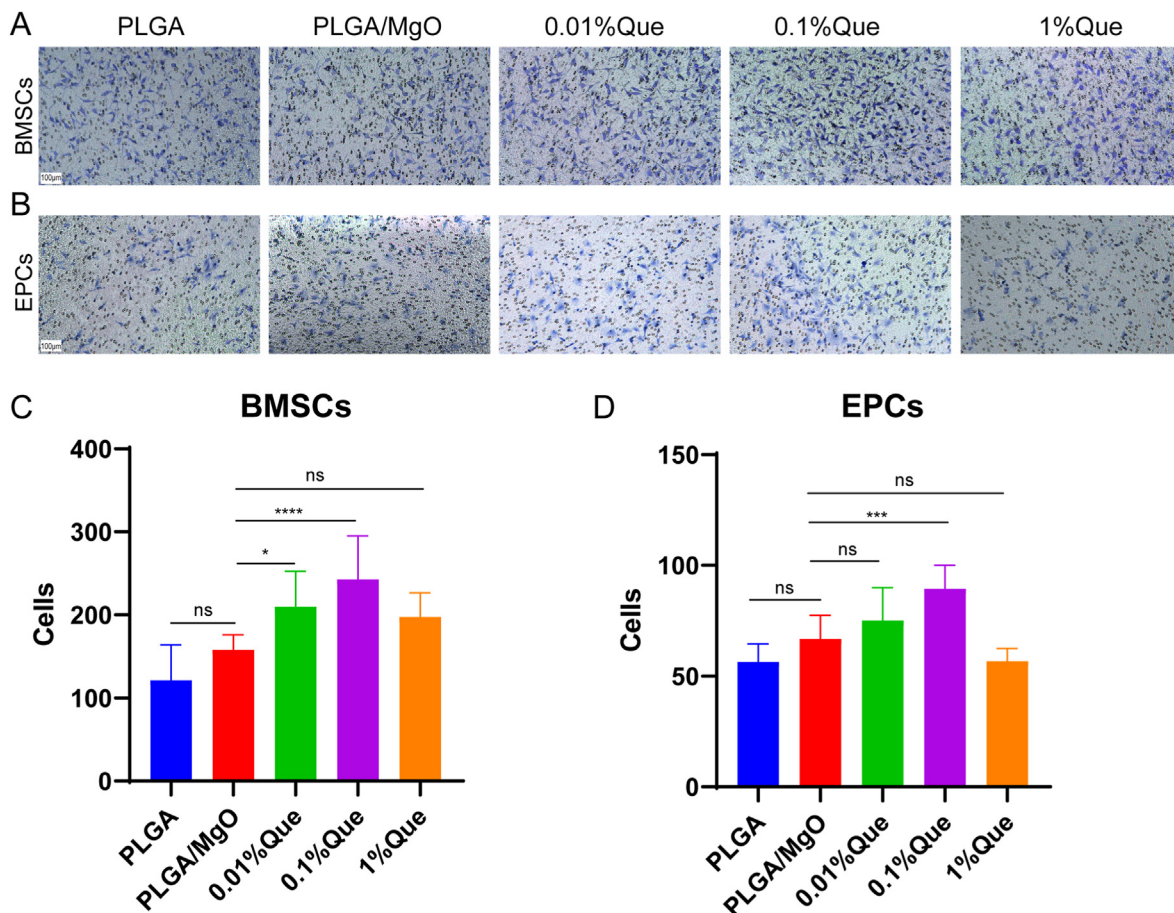
Fig. 3. PLGA/MgO/Que increased cell migration. (A) and (B), Cultured in membranes immersing extracts, Proper concentration of PLGA/MgO/Que membranes increasing migration in BMSCs(A) and EPCs(B); (C) and (D), Statistical analysis of cell migration of each group in BMSCs(C) and EPCs(D) (N = 3); *$p < 0.05$, **$p < 0.01$, ***$p < 0.001$, ****$p < 0.0001$.

showed higher expression of Vwf ($p < 0.05$). Compared with PLGA/MgO, 0.1% showed increasing expression of Vegfa ($p < 0.01$) and Vwf ($p < 0.05$). However, 1% Que showed decreased expression of Vwf ($p < 0.05$) (Fig. 5C). By immunoblotting, we also observed highest expression of eNOS in 0.1% Que (Fig. 5D).

By immunofluorescence staining, the cytoskeleton of 0.1% Que and 0.01% Que groups became slender and arranged in rings, similar to the migration behavior of tubules on matrix glue in vitro (Fig. 5E). We also observed highest fluorescence intensity in 0.1% Que stained with eNOS and CD31 (Fig. 5F), suggesting that 0.1% Que showed the best angiogenesis function however 1% Que might inhibit angiogenesis.

3.6. Evaluation of biocompatibility and angiogenesis of PLGA/MgO/Que in subcutaneous implantation model

In studies above, 0.1% Que showed the best angiogenesis and osteogenesis. Thus, we used a rat subcutaneous implantation model to evaluate the biocompatibility and angiogenesis of PLGA, PLGA/MgO and 0.1% Que. Samples were collected 14 days after surgery. There were no signs of inflammatory fibrosis. By H&E and Masson staining, good interface combination between materials and tissues was displayed and no obvious inflammatory reaction was noted, which suggested excellent biocompatibility. Neovascularization could be observed in all groups; however, 0.1% Que showed the most neovascularization. By H&E and Masson staining as well as CD31 immunofluorescence staining, we observed highest number and density of neovascularization in 0.1% Que (Fig. 6).

3.7. Evaluation of repair effect of PLGA/MgO/Que in rat skull defect model

We used the rat skull defect model to evaluate the effect of PLGA, PLGA/MgO and 0.1% Que on promoting bone defect repairing. Samples for micro-CT scanning and reconstruction (Fig. 7A) were collected 8 weeks after surgery. 0.1% Que showed the best repair function among the three groups in both micro-CT scanning and Bone volume, BV/TV analysis (Fig. 7B). As shown in Figure, PLGA demonstrated the lowest bone repair effect with a bone volume fraction of 26.34%. The PLGA/MgO membrane group showed a better bone repair effect than pure PLGA ($p < 0.01$), with a bone volume fraction of 37.83%. Compared with PLGA/MgO, the bone volume fraction of Que nanofiber membrane was 51.51%, which had the best bone repair effect ($p < 0.01$). Similar results were shown in neogenesis bone volume in bone defects areas.

Importantly, these results were consistent with the trend of micro-CT.

Histological examination was investigated to further verify the microscopic details of the defect area. As shown in H&E and Masson trichrome staining images, compared with the control group, the quercetin and MgO groups had fewer bone defect areas than the control group. Meanwhile, Masson staining showed that the collagen fibers in the PLGA group were very sparse. In contrast, the collagen fibers in both the MgO and quercetin groups were greater than those in the PLGA group. At the same time, OCN (osteogenic marker) immunohistochemical staining also showed that PLGA/MgO/Que can promote the bone formation, consistent with the CT results. CD31 (angiogenic marker) verified the angiogenic effect of MgO. Both PLGA/MgO and PLGA/MgO/Que groups showed better angiogenesis than PLGA alone, consistent with in vitro
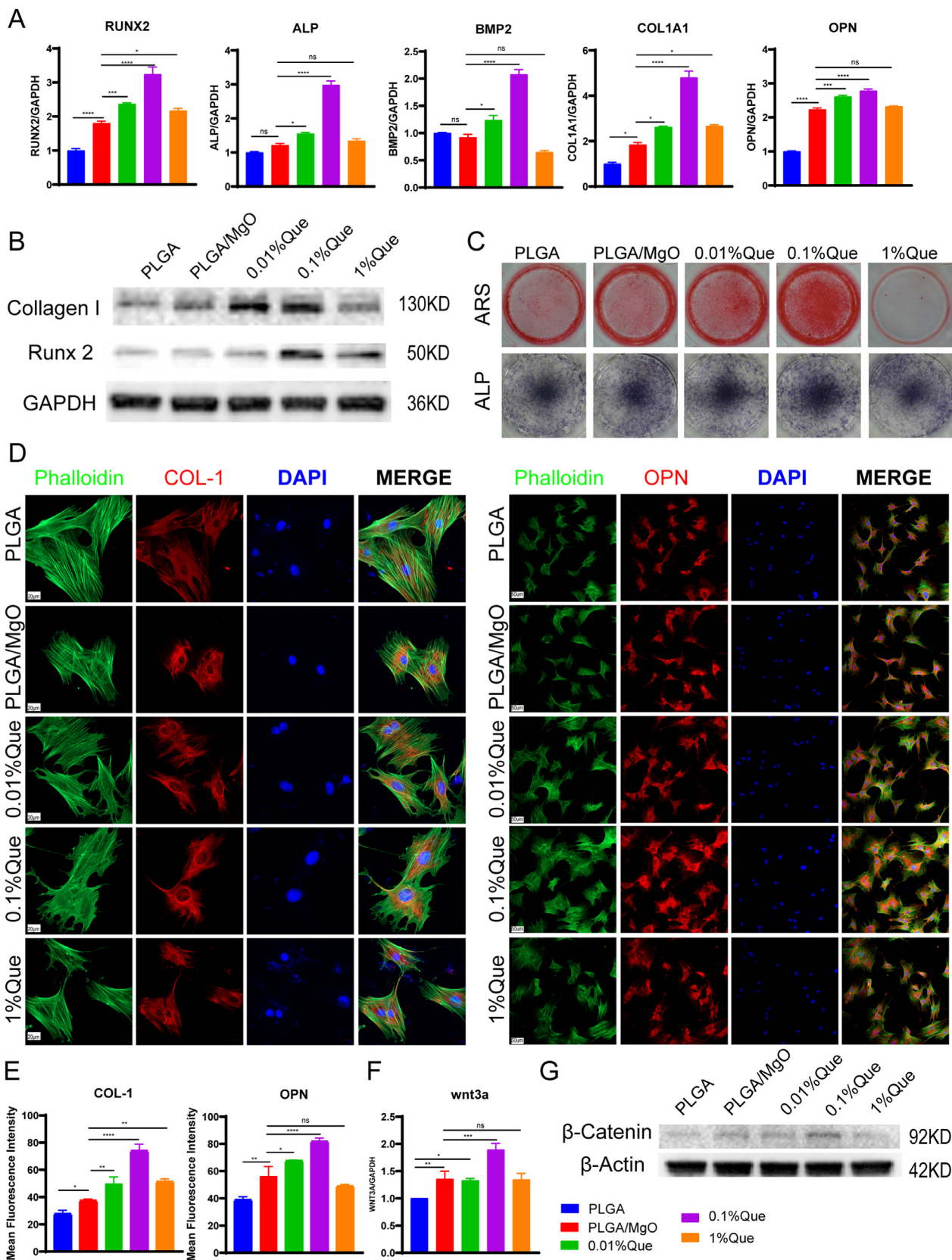
Fig. 4. PLGA/MgO/Que increased osteogenesis via Wnt/β-catenin signaling pathway. (A) Proper concentration of PLGA/MgO/Que increased the expression of osteogenesis associated genes including RUNX2, ALP, BMP2, COL1A1 and OPN in BMSCs; (B) in BMSCs, the expression of collagen I and Runx2 increased in Que membranes immersing medium; (C) Alizarin Red stain and ALP Stain showed Que could promote osteogenesis in 0.1% concentration; (D) cultured in membranes immersing extracts, Que increasing the expression of Collagen I and OPN, the scale is 20 μm (left) and 50 μm (right); (E) Statistical analysis of fluorescence intensity of Collagen I (left) and OPN (right); (F) and (G) 0.1% Que immersing medium increased the expression of Wnt3a and non-phospho catenin in BMSCs; *$p < 0.05$, **$p < 0.01$, ***$p < 0.001$, ****$p < 0.0001$.
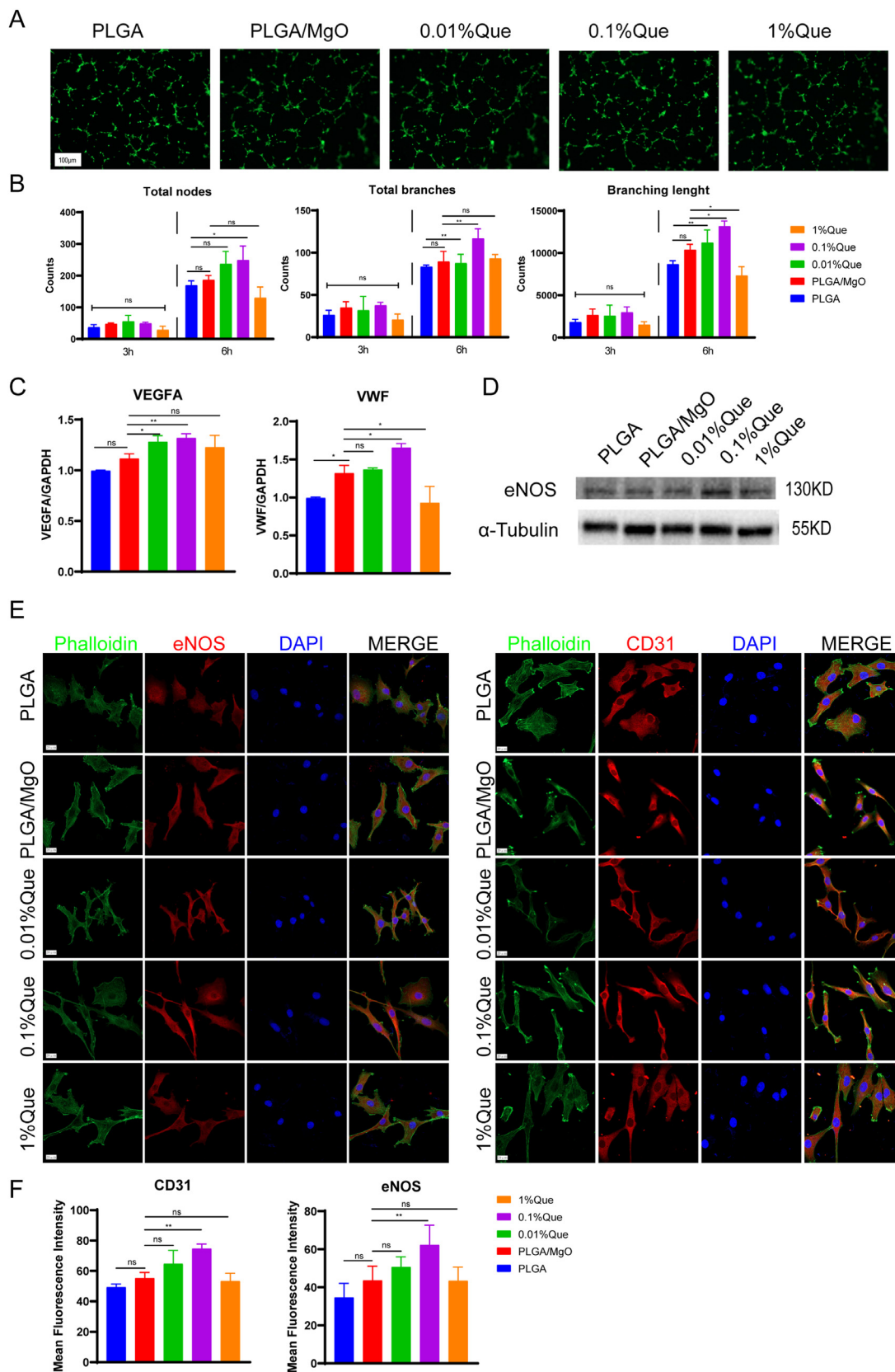
Fig. 5. PLGA/MgO/Que increased angiogenesis. (A) and (B), Stained with phalloidin (A), we found total nodes, total branches and branching length increased in EPCS cultured with 0.1%Que immersing medium (B); (C) and (D), 0.1% Que increased the expression of VEGFA, VWF (C) and eNOS (D); (E) and (F), tested by immu-nofluorescence, 0.1% Que increased the expression of eNOS and CD31, the scale is 20 μM; *$p < 0.05$, **$p < 0.01$, ***$p < 0.001$, ****$p < 0.0001$.
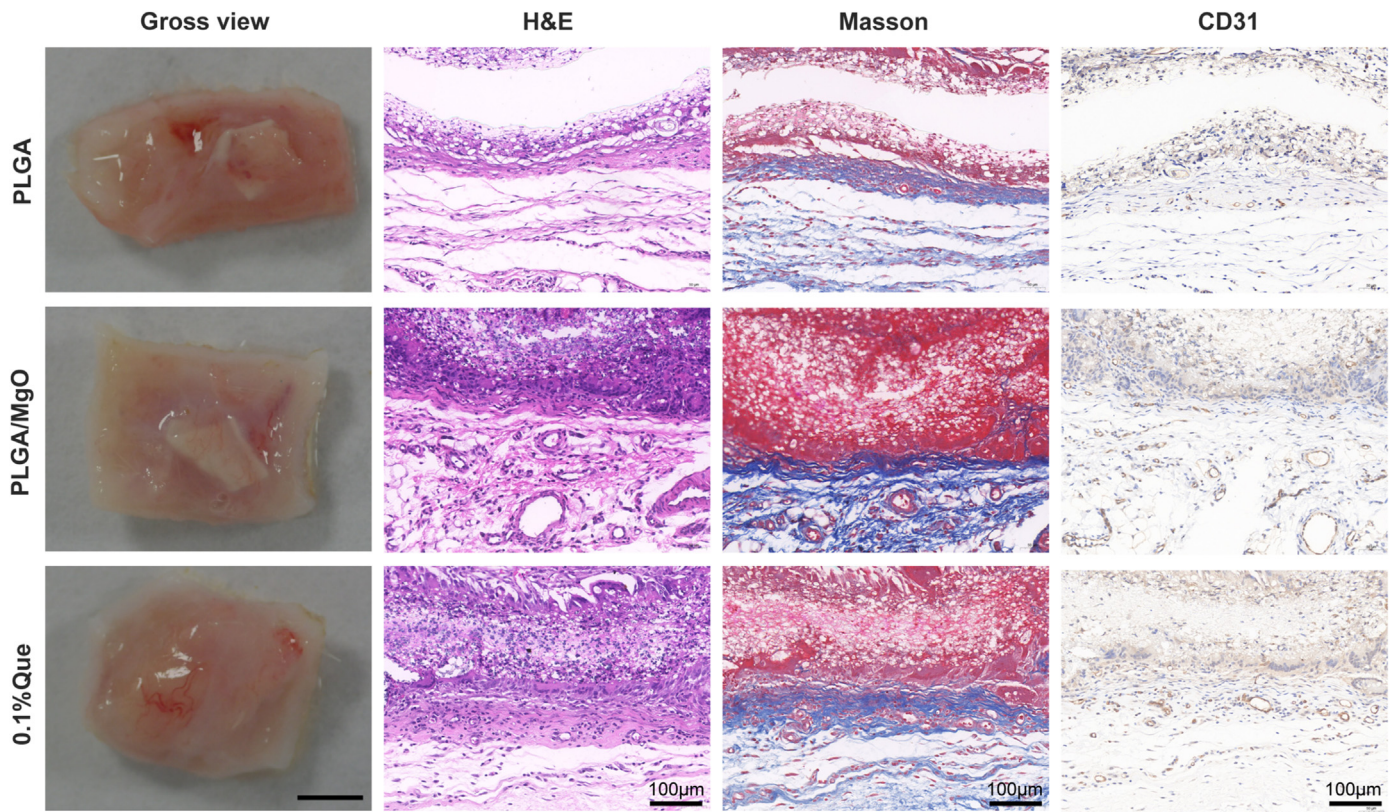
Fig. 6. 0.1%Que membranes increased angiogenesis in subcutaneous implantation model Under gross view, it is observed that 0.1% Que group showed more vessels than PLGA and PLGA/MgO groups; no profound fibrous scar was found in each group, indicating excellent biocompatibility of groups; by H&E and Masson staining, as well as histochemistry staining of CD31, we observed more neovascularization in 0.1% Que group, (N = 3).
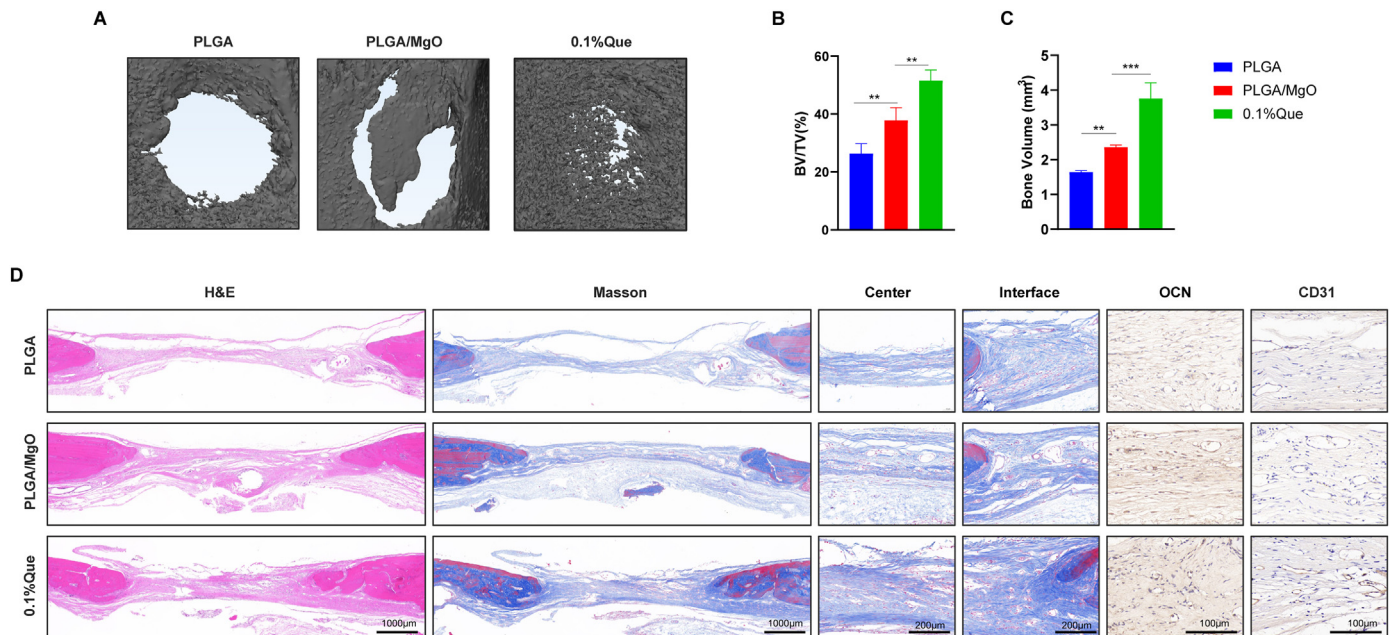
Fig. 7. 0.1%Que membranes accelerated bone repair in rat skull defect model (A) Scanned by micro-CT, 0.1%Que membranes showed the best repairing effects in rat skull defect model; (B) by BV/TV analysis, 0.1%Que membranes showed better repairing effects than other two groups; (C) 0.1%Que membranes showed the most neogenesis bone volume in bone defects areas; (D) by H&E, Masson staining and histochemistry staining of CD31 and OCN, we observed better repairing of bone in 0.1%Que membrane group (N = 3), $*p < 0.05$, $**p < 0.01$, $***p < 0.001$, $****p < 0.0001$.

tube formation experiments (Fig. 7C). As neurovascular network formation was highly associated with bone repair, we conducted immunofluorescence staining in bone defects area. 0.1% Que showed the highest expression of CD31 (angiogenic marker) and β3-tubulin (neuron marker) in bone defect areas, which indicating an increasing of neurovascular network formation (Figure S2).

4. Discussion

In this study, nano artificial periosteum was prepared by electrospinning with PLGA as the main substrate. MgO and Que were used as the main active factors to promote bone regeneration. The biocompatibility, osteogenesis and angiogenesis of the nano artificial periosteum was evaluated. Through SEM, we found that PLGA/MgO/Que nanofiber membrane had a highly porous surface and microstructure, which is conducive to cell adhesion and inward growth and provides necessary space for neovascularization.

PLGA/MgO/Que artificial periosteum showed no cytotoxicity and there was no obvious fibrosis in the subcutaneous tissue of the material implantation site on the subcutaneous animal model, suggesting good biocompatibility. Estimating rat skull defect model and subcutaneous implantation model, the degradation time of membranes was between 2 and 8 weeks, which seemed a short sustaining time for artificial periosteum caused by fast degeneration of PLGA [31]. With the degradation of artificial periosteum, MgO and Que were released. To improve the degradation rate of the PLGA/MgO/Que films, other polymers with slower degradation rate such as PCL could be added as the main substrate in future studies. Considering hydrophobic characteristics of PLGA, low solubility of MgO in water and Que fat-soluble characteristics, the water contact angle of the membrane further increased after adding MgO and Que, resulting in poor hydrophilicity of the spinning membrane. However, the decrease of hydrophilicity may also slow down the degradation rate. PLGA is usually hydrolyzed into lactic acid and glycolic acid, which can neutralize alkaline MgO nanoparticles, thus helping bone regeneration and slow down the degradation rate [30].

MgO nanoparticles can release Mg^{2+} in vivo and promote bone regeneration by affecting the secretion of CGRP by local neurons, or by TRPM7-mediated macrophage immune regulation [32–34]. Mg^{2+} has been proved to play a crucial role in osteogenesis and angiogenesis [35–38]. In addition to bone induction, a functional microvascular network was very important for bone regeneration. In the process of bone regeneration, osteogenesis and angiogenesis are coupled and promote each other [39], and one of the important roles of periosteum is to ensure blood and nutrition supply for bone tissue. Therefore, well-designed artificial periosteum should have the coupling effect of "osteogenesis-angiogenesis". Some magnesium-containing scaffolds also confirmed the promoting effect of "osteogenesis-angiogenesis" coupling on bone regeneration [9,16,40]. A sustainable releasing of Mg^{2+} was proved in artificial periosteum we constructed in this project. Our results also suggest that artificial periosteum containing MgO can promote stem cell migration and osteogenic differentiation in vitro, as well as EPCs migration and tube formation in vitro. Further, in vivo experiments also verified the role of promoting bone and angiogenesis.

Que promoted osteogenesis and helped to maintain bone homeostasis. However, the role of Que in angiogenesis was controversial. In HUVEC, Que (>136 μM or 10 μg/mL) inhibited cell migrations and tube formation. Que (>136 μM or 10 μg/mL) also played a role in anti-tumor activity by suppressing angiogenesis [41,42]. In other studies, Que-containing nHA bioceramic microspheres promoted osteogenesis and angiogenesis [43]. The concentration that promoted osteogenesis was much lower than the concentration that inhibited angiogenesis in tumors [18], suggesting that low concentration Que helped osteogenesis and angiogenesis. This is similar to the observations in this study where 0.01% and 0.1% Que showed coupling effect of "osteogenesis-angiogenesis" in a dosage-dependent manner, but 1% Que suppressed the osteogenesis and angiogenesis. It provided directions for further study of Que containing biomaterials.

Peripheral nerves participated in bone development and repair by secreting neurotransmitters, neuropeptides etc. [44]. The lack of neo-neurovascular network in bone implants might be one of the main reasons for the delayed or damaged recovery of bone defects [45]. Good orthopedic biomaterials should promote the repair of neurovascular network in bone defects. Previous studies also reported Que could promote axonal regeneration of peripheral nerve and functional recovery of nerve [46,47]. In this study, we found 0.1% Que membranes could promote neurovascular network formation in bone defect area. Que and MgO have effects on osteogenesis and angiogenesis independently [17, 18,48]. Compared with PLGA/MgO, PLGA/MgO/0.1% Que showed superior osteogenesis and angiogenesis, indicating Que at an appropriate concentration can enhance osteogenic angiogenesis coupling effect of MgO, which displaying synergy between Que and MgO.

Wnt/β-Catenin signaling pathway is a canonical osteogenic pathway. An up regulation of Wnt3a could stimulate β-catenin and increasing osteogenesis [49]. Both Que and Mg^{2+} could help bone defect repair by activating Wnt/β-catenin signaling pathway [22,48,50]. Thus, in this study we explored possible synergistic effect of both Que and Mg^{2+}. Compared with PLGA, MgO could increasing the expression of Wnt3a as we expected. By adding 0.1% Que, we observed extra increasing of Wnt3a in 0.1% Que group. 0.1% Que also showed the highest expression of β-catenin. We suggested that PLGA/MgO/0.1% Que artificial periosteum promoted bone repair through activating Wnt/β-catenin pathways. However, further study on the regulation of Wnt3a and the specific role of MgO or Que in upregulation of Wnt/β-catenin will be carried out in our subsequent studies.

5. Conclusion

Artificial periosteum of PLGA/MgO/Que were prepared in this study. Appropriate concentrations of Que cooperate with MgO exerted osteogenic−angiogenic coupling effect, accelerating the repair of bone defects through activation of the Wnt/β-catenin signaling pathway. This suggests that an appropriate concentration of PLGA/MgO/Que artificial periosteum might show a variety of biological activities and has potential for use as artificial periosteum.

Credit author statement

Xi He: Conceptualization; Data curation; Formal analysis; Funding acquisition; Investigation; Visualization; Roles/Writing - original draft, **Wenbin Liu**: Conceptualization; Data curation; Writing – review & editing, **Yanling Liu**: Investigation; Methodology, **Kai Zhang**: Investigation; Methodology, **Yan Sun**: Investigation; Methodology, **Pengfei Lei**: Conceptualization; Data curation; Funding acquisition; Writing – review & editing, **Yihe Hu**: Conceptualization; Data curation; Funding acquisition; Writing – review & editing

Data availability statement

Data is available from the corresponding authors on reasonable request.

Declaration of competing interest

The authors declare that they have no known competing financial interests or personal relationships that could have appeared to influence the work reported in this paper.

Acknowledgements

Appendix A. Supplementary data

Supplementary data to this article can be found online at https://doi.org/10.1016/j.mtbio.2022.100348.

References

[1] T. Wang, Y. Zhai, M. Nuzzo, X. Yang, Y. Yang, X. Zhang, Layer-by-layer nanofiber-enabled engineering of biomimetic periosteum for bone repair and reconstruction, Biomaterials 182 (2018) 279–288.
[2] X. Zhang, H.A. Awad, R.J. O'Keefe, R.E. Guldberg, E.M. Schwarz, A perspective: engineering periosteum for structural bone graft healing, Clin. Orthop. Relat. Res. 466 (8) (2008) 1777–1787.
[3] B. Gao, R. Deng, Y. Chai, H. Chen, B. Hu, X. Wang, S. Zhu, Y. Cao, S. Ni, M. Wan, L. Yang, Z. Luo, X. Cao, Macrophage-lineage TRAP+ cells recruit periosteum-derived cells for periosteal osteogenesis and regeneration, J. Clin. Invest. 129 (6) (2019) 2578–2594.
[4] M.L. Knothe Tate, S. Dolejs, S.H. McBride, R. Matthew Miller, U.R. Knothe, Multiscale mechanobiology of de novo bone generation, remodeling and adaptation of autograft in a common ovine femur model, J. Mech. Behav. Biomed. Mater. 4 (6) (2011) 829–840.
[5] A.R. Lozada-Gallegos, J. Letechipia-Moreno, I. Palma-Lara, A.A. Montero, G. Rodríguez, F. Castro-Muñozledo, M.A. Cornejo-Cortés, M.L. Juárez-Mosqueda, Development of a bone nonunion in a noncritical segmental tibia defect model in sheep utilizing interlocking nail as an internal fixation system, J. Surg. Res. 183 (2) (2013) 620–628.
[6] W. Zhang, N. Wang, M. Yang, T. Sun, J. Zhang, Y. Zhao, N. Huo, Z. Li, Periosteum and development of the tissue-engineered periosteum for guided bone regeneration, J. Orthop. Translat. 33 (2022) 41–54.
[7] J. Lin, L. Liu, S. Huang, W. Zheng, H. Liu, Z. Bai, K. Jiang, X. Wang, PCL nanofibrous incorporating unique matrix fusion protein adsorbed mesoporous bioactive glass for bone tissue engineering, Int. J. Biol. Macromol. 208 (2022) 136–148.
[8] H.A. Owida, J.I. Al-Nabulsi, F. Alnaimat, M. Al-Ayyad, N.M. Turab, A. Al Sharah, M. Shakur, Recent applications of electrospun nanofibrous scaffold in tissue engineering, Appl. Bionics Biomechanics 2022 (2022), 1953861.
[9] X. Zhang, W. Liu, J. Liu, Y. Hu, H. Dai, Poly-ε-caprolactone/Whitlockite electrospun bionic membrane with an osteogenic-angiogenic coupling effect for periosteal regeneration, ACS Biomater. Sci. Eng. 7 (7) (2021) 3321–3331.
[10] H.E. Owston, K.M. Moisley, G. Tronci, S.J. Russell, P.V. Giannoudis, E. Jones, Induced periosteum-mimicking membrane with cell barrier and multipotential stromal cell (MSC) homing functionalities, Int. J. Mol. Sci. 21 (15) (2020).
[11] P. Ganguly, E. Jones, V. Panagiotopoulou, A. Jha, M. Blanchy, S. Antimisiaris, M. Anton, B. Dhuiège, M. Marotta, N. Marjanovic, E. Panagiotopoulos, P. Giannoudis, Electrospun and 3D printed polymeric materials for one-stage critical-size long bone defect regeneration inspired by the Masquelet technique: recent Advances, Injury (2022), https://doi.org/10.1016/j.injury.2022.02.036. In press.
[12] Z. Lin, D. Shen, W. Zhou, Y. Zheng, T. Kong, X. Liu, S. Wu, P.K. Chu, Y. Zhao, J. Wu, K.M.C. Cheung, K.W.K. Yeung, Regulation of extracellular bioactive cations in bone tissue microenvironment induces favorable osteoimmune conditions to accelerate in situ bone regeneration, Bioact. Mater. 6 (8) (2021) 2315–2330.
[13] Z. Yuan, Z. Wan, P. Wei, X. Lu, J. Mao, Q. Cai, X. Zhang, X. Yang, Dual-Controlled release of Icariin/Mg(2+) from biodegradable microspheres and their synergistic upregulation effect on bone regeneration, Adv. Healthc Mater. 9 (11) (2020), e2000211.
[14] Z. Yuan, P. Wei, Y. Huang, W. Zhang, F. Chen, X. Zhang, J. Mao, D. Chen, Q. Cai, X. Yang, Injectable PLGA microspheres with tunable magnesium ion release for promoting bone regeneration, Acta Biomater. 85 (2019) 294–309.
[15] Y. Chen, W. Sheng, J. Lin, C. Fang, J. Deng, P. Zhang, M. Zhou, P. Liu, J. Weng, F. Yu, D. Wang, B. Kang, H. Zeng, Magnesium oxide nanoparticle coordinated phosphate-functionalized chitosan injectable hydrogel for osteogenesis and angiogenesis in bone regeneration, ACS Appl. Mater. Interfaces 14 (6) (2022) 7592–7608.
[16] C.C. Coelho, T. Padrão, L. Costa, M.T. Pinto, P.C. Costa, V.F. Domingues, P.A. Quadros, F.J. Monteiro, S.R. Sousa, The antibacterial and angiogenic effect of magnesium oxide in a hydroxyapatite bone substitute, Sci. Rep. 10 (1) (2020), 19098.
[17] P. Shen, W. Lin, X. Deng, X. Ba, L. Han, Z. Chen, K. Qin, Y. Huang, S. Tu, Potential implications of quercetin in autoimmune diseases, Front. Immunol. 12 (2021), 689044.
[18] S.K. Wong, K.Y. Chin, S. Ima-Nirwana, Quercetin as an agent for protecting the bone: a review of the current evidence, Int. J. Mol. Sci. 21 (17) (2020).
[19] X.G. Pang, Y. Cong, N.R. Bao, Y.G. Li, J.N. Zhao, Quercetin stimulates bone marrow mesenchymal stem cell differentiation through an estrogen receptor-mediated pathway, BioMed Res. Int. 2018 (2018), 4178021.
[20] N. Wang, L. Wang, J. Yang, Z. Wang, L. Cheng, Quercetin Promotes Osteogenic Differentiation and Antioxidant Responses of Mouse Bone Mesenchymal Stem Cells through Activation of the AMPK/SIRT1 Signaling Pathway, Phytother Res, 2021.
[21] C. Zhou, Y. Lin, Osteogenic differentiation of adipose-derived stem cells promoted by quercetin, Cell Prolif 47 (2) (2014) 124–132.
[22] C. Guo, R.J. Yang, K. Jang, X.L. Zhou, Y.Z. Liu, Protective effects of pretreatment with quercetin against lipopolysaccharide-induced apoptosis and the inhibition of osteoblast differentiation via the MAPK and Wnt/β-catenin pathways in MC3T3-E1 cells, Cell. Physiol. Biochem. 43 (4) (2017) 1547–1561.
[23] Z. Yuan, J. Min, Y. Zhao, Q. Cheng, K. Wang, S. Lin, J. Luo, H. Liu, Quercetin rescued TNF-alpha-induced impairments in bone marrow-derived mesenchymal stem cell osteogenesis and improved osteoporosis in rats, Am J Transl Res 10 (12) (2018) 4313–4321.
[24] A.A. Welch, A.C. Hardcastle, The effects of flavonoids on bone, Curr. Osteoporos. Rep. 12 (2) (2014) 205–210.
[25] B. Fernandez-Rojas, G. Gutierrez-Venegas, Flavonoids exert multiple periodontic benefits including anti-inflammatory, periodontal ligament-supporting, and alveolar bone-preserving effects, Life Sci. 209 (2018) 435–454.
[26] A.M. Preethi, J.R. Bellare, Concomitant effect of quercetin- and magnesium-doped calcium silicate on the osteogenic and antibacterial activity of scaffolds for bone regeneration, Antibiot. (Basel) 10 (10) (2021).
[27] Z. Lin, J. Wu, W. Qiao, Y. Zhao, K.H.M. Wong, P.K. Chu, L. Bian, S. Wu, Y. Zheng, K.M.C. Cheung, F. Leung, K.W.K. Yeung, Precisely controlled delivery of magnesium ions thru sponge-like monodisperse PLGA/nano-MgO-alginate core-shell microsphere device to enable in-situ bone regeneration, Biomaterials 174 (2018) 1–16.
[28] R. Ren, J. Guo, J. Shi, Y. Tian, M. Li, H. Kang, PKM2 regulates angiogenesis of VR-EPCs through modulating glycolysis, mitochondrial fission, and fusion, J. Cell. Physiol. 235 (9) (2020) 6204–6217.
[29] X. He, Z. Huang, W. Liu, Y. Liu, H. Qian, T. Lei, L. Hua, Y. Hu, Y. Zhang, P. Lei, Electrospun polycaprolactone/hydroxyapatite/ZnO films as potential biomaterials for application in bone-tendon interface repair, Colloids Surf. B Biointerfaces 204 (2021), 111825.
[30] X. Xia, J. Huang, J. Wei, S. Jin, Q. Zou, Y. Zuo, J. Li, Y. Li, Magnesium oxide regulates the degradation behaviors and improves the osteogenesis of poly(lactide-co-glycolide) composite scaffolds, Compos. Sci. Technol. 222 (2022), 109368.
[31] Z. Pan, J. Ding, Poly(lactide-co-glycolide) porous scaffolds for tissue engineering and regenerative medicine, Interface Focus 2 (3) (2012) 366–377.
[32] W. Qiao, K.H.M. Wong, J. Shen, W. Wang, J. Wu, J. Li, Z. Lin, Z. Chen, J.P. Matinlinna, Y. Zheng, S. Wu, X. Liu, K.P. Lai, Z. Chen, Y.W. Lam, K.M.C. Cheung, K.W.K. Yeung, TRPM7 kinase-mediated immunomodulation in macrophage plays a central role in magnesium ion-induced bone regeneration, Nat. Commun. 12 (1) (2021) 2885.
[33] Y. Zhang, J. Xu, Y.C. Ruan, M.K. Yu, M. O'Laughlin, H. Wise, D. Chen, L. Tian, D. Shi, J. Wang, S. Chen, J.Q. Feng, D.H. Chow, X. Xie, L. Zheng, L. Huang, S. Huang, K. Leung, N. Lu, L. Zhao, H. Li, D. Zhao, X. Guo, K. Chan, F. Witte, H.C. Chan, Y. Zheng, L. Qin, Implant-derived magnesium induces local neuronal production of CGRP to improve bone-fracture healing in rats, Nat. Med. 22 (10) (2016) 1160–1169.
[34] L. Ye, J. Xu, J. Mi, X. He, Q. Pan, L. Zheng, H. Zu, Z. Chen, B. Dai, X. Li, Q. Pang, L. Zou, L. Zhou, L. Huang, W. Tong, G. Li, L. Qin, Biodegradable magnesium combined with distraction osteogenesis synergistically stimulates bone tissue regeneration via CGRP-FAK-VEGF signaling axis, Biomaterials 275 (2021), 120984.
[35] Y. Zhang, T. Lin, H. Meng, X. Wang, H. Peng, G. Liu, S. Wei, Q. Lu, Y. Wang, A. Wang, W. Xu, H. Shao, J. Peng, 3D gel-printed porous magnesium scaffold coated with dibasic calcium phosphate dihydrate for bone repair in vivo, J. Orthop. Translat. 33 (2022) 13–23.
[36] Y. Li, Q. Pan, J. Xu, X. He, H.A. Li, D.A. Oldridge, G. Li, L. Qin, Overview of methods for enhancing bone regeneration in distraction osteogenesis: potential roles of biometals, J. Orthop. Translat. 27 (2021) 110–118.
[37] M. Wang, Y. Feng, K. Yuan, S. Yang, T. Tang, Dual-functional hybrid quaternized chitosan/Mg/alginate dressing with antibacterial and angiogenic potential for diabetic wound healing, J. Orthop. Translat. 30 (2021) 6–15.
[38] D.H.K. Chow, J. Wang, P. Wan, L. Zheng, M.T.Y. Ong, L. Huang, W. Tong, L. Tan, K. Yang, L. Qin, Biodegradable magnesium pins enhanced the healing of transverse patellar fracture in rabbits, Bioact. Mater. 6 (11) (2021) 4176–4185.
[39] Y. Yang, T. Xu, Q. Zhang, Y. Piao, H.P. Bei, X. Zhao, Biomimetic, stiff, and adhesive periosteum with osteogenic-angiogenic coupling effect for bone regeneration, Small 17 (14) (2021), e2006598.
[40] Y. Lai, Y. Li, H. Cao, J. Long, X. Wang, L. Li, C. Li, Q. Jia, B. Teng, T. Tang, J. Peng, D. Eglin, M. Alini, D.W. Grijpma, G. Richards, L. Qin, Osteogenic magnesium incorporated into PLGA/TCP porous scaffold by 3D printing for repairing challenging bone defect, Biomaterials 197 (2019) 207–219.
[41] S. Esteghlal, M.J. Mokhtari, Z. Beyzaei, Quercetin can inhibit angiogenesis via the down regulation of MALAT1 and MIAT LncRNAs in human umbilical vein endothelial cells, Int. J. Prev. Med. 12 (2021) 59.
[42] Y. Liu, Z.G. Tang, J.Q. Yang, Y. Zhou, L.H. Meng, H. Wang, C.L. Li, Low concentration of quercetin antagonizes the invasion and angiogenesis of human glioblastoma U251 cells, OncoTargets Ther. 10 (2017) 4023–4028.
[43] Y. Zhou, Y. Wu, W. Ma, X. Jiang, A. Takemra, M. Uemura, L. Xia, K. Lin, Y. Xu, The effect of quercetin delivery system on osteogenesis and angiogenesis under osteoporotic conditions, J. Mater. Chem. B 5 (3) (2017) 612–625.
[44] Q.Q. Wan, W.P. Qin, Y.X. Ma, M.J. Shen, J. Li, Z.B. Zhang, J.H. Chen, F.R. Tay, L.N. Niu, K. Jiao, Crosstalk between bone and nerves within bone, Adv. Sci. 8 (7) (2021), 2003390.
[45] B.P. Dos Santos, B. Garbay, M. Fenelon, M. Rosselin, E. Garanger, S. Lecommandoux, H. Oliveira, J. Amédée, Development of a cell-free and growth factor-free hydrogel capable of inducing angiogenesis and innervation after subcutaneous implantation, Acta Biomater. 99 (2019) 154–167.
[46] M.M. Chen, Z.Q. Yin, L.Y. Zhang, H. Liao, Quercetin promotes neurite growth through enhancing intracellular cAMP level and GAP-43 expression, Chin. J. Nat. Med. 13 (9) (2015) 667–672.
[47] Y. Wang, M. Xiong, M. Wang, H. Chen, W. Li, X. Zhou, Quercetin promotes locomotor function recovery and axonal regeneration through induction of

autophagy after spinal cord injury, Clin. Exp. Pharmacol. Physiol. 48 (12) (2021) 1642–1652.

[48] C.C. Hung, A. Chaya, K. Liu, K. Verdelis, C. Sfeir, The role of magnesium ions in bone regeneration involves the canonical Wnt signaling pathway, Acta Biomater. 98 (2019) 246–255.

[49] X. Chen, K. Yang, P. Sun, R. Zhao, B. Liu, P. Lu, Exercise improves bone formation by upregulating the Wnt3a/β-catenin signalling pathway in type 2 diabetic mice, Diabetol. Metab. Syndrome 13 (1) (2021) 116.

[50] J. Xu, P. Hu, X. Zhang, J. Chen, J. Wang, J. Zhang, Z. Chen, M.K. Yu, Y.W. Chung, Y. Wang, X. Zhang, Y. Zhang, N. Zheng, H. Yao, J. Yue, H.C. Chan, L. Qin, Y.C. Ruan, Magnesium implantation or supplementation ameliorates bone disorder in CFTR-mutant mice through an ATF4-dependent Wnt/β-catenin signaling, Bioact. Mater. 8 (2022) 95–108.